



INSTITUT DE FRANCE
Académie des sciences

Comptes Rendus

Chimie

Thibaut Baron, Ximena Zarate, Yoan Hidalgo-Rosa, Michael Zambrano-Angulo, Kevin Mall-Haidaraly, Ricardo Pino-Rios, Yann Pellegrin, Fabrice Odobel and Gloria Cárdenas-Jirón

Zinc phthalocyanine absorbance in the near-infrared with application for transparent and colorless dye-sensitized solar cells

Volume 24, Special Issue S3 (2021), p. 157-170


Published online: 15 October 2021

Issue date: 16 December 2021

<https://doi.org/10.5802/crchim.113>

Part of Special Issue: MAPYRO: the French Fellowship of the Pyrrolic Macrocyclic Ring

Guest editors: Bernard Boitrel (Institut des Sciences Chimiques de Rennes, CNRS-Université de Rennes 1, France) and Jean Weiss (Institut de Chimie de Strasbourg, CNRS-Université de Strasbourg, France)

 This article is licensed under the
CREATIVE COMMONS ATTRIBUTION 4.0 INTERNATIONAL LICENSE.
<http://creativecommons.org/licenses/by/4.0/>



Les Comptes Rendus. Chimie sont membres du
Centre Mersenne pour l'édition scientifique ouverte
www.centre-mersenne.org
e-ISSN : 1878-1543



MAPYRO: the French Fellowship of the Pyrrolic Macrocyclic Ring / MAPYRO: la communauté française des macrocycles pyrroliques

Zinc phthalocyanine absorbance in the near-infrared with application for transparent and colorless dye-sensitized solar cells

Thibaut Baron^a, Ximena Zarate^{*,b}, Yoan Hidalgo-Rosa^{*,c},
Michael Zambrano-Angulo^d, Kevin Mall-Haidaraly^a, Ricardo Pino-Rios^d,
Yann Pellegrin^{*,a}, Fabrice Odobel^{*,a} and Gloria Cárdenas-Jirón^{*,d}

^a Université de Nantes, CNRS, CEISAM UMR 6230, F-44000 Nantes, France

^b Instituto de Ciencias Químicas Aplicadas, Facultad de Ingeniería, Universidad Autónoma de Chile, Santiago, Chile

^c Doctorado en Fisicoquímica Molecular, Universidad Andres Bello, Santiago, Chile

^d Laboratory of Theoretical Chemistry, Faculty of Chemistry and Biology, University of Santiago de Chile (USACH), Santiago, Chile

E-mails: thibaut.baron@univ-nantes.fr (T. Baron), ximena.zarate@uautonoma.cl (X. Zarate), yoanhrj@gmail.com (Y. Hidalgo-Rosa), michael.zambrano@usach.cl (M. Zambrano-Angulo), kevin.mallhaidaraly@gmail.com (K. Mall-Haidaraly), ricardo.pino@usach.cl (R. Pino-Rios), Yann.Pellegrin@univ-nantes.fr (Y. Pellegrin), Fabrice.Odobel@univ-nantes.fr (F. Odobel), gloria.cardenas@usach.cl (G. Cárdenas-Jirón)

Abstract. Transparent and colorless solar cells are attractive new photovoltaic devices as they could bring new opportunities to harness sunlight energy and particularly for their integration in windows. In this work, a new zinc phthalocyanine was synthesized and investigated as sensitizer in dye-sensitized solar cell (DSSC) for this purpose. The zinc phthalocyanine features a benzoic acid anchoring group and six thio(4-tertbutylphenyl) substituents in α position of the phthalocyanine. The dye was characterized by absorption and emission spectroscopy and by electrochemistry. The physico-chemical properties show that the dye fulfills the criteria for such an application. A detailed computational study indicates that the electronic communication with TiO₂ conduction is weak owing to the absence of overlapping of the wavefunctions of the dye with those of the TiO₂ semiconductor. The photovoltaic performances of the zinc phthalocyanine were measured in TiO₂-based DSSC that revealed inefficient electron injection, which certainly can be explained by the weak electronic coupling of the dye with TiO₂ that limits electron injection efficiency. A strategy is proposed to make better-performing sensitizers.

Keywords. Phthalocyanine, Solar cell, Solar energy, Dye sensitized solar cell, Near infrared.

Available online 15th October 2021

* Corresponding authors.

1. Introduction

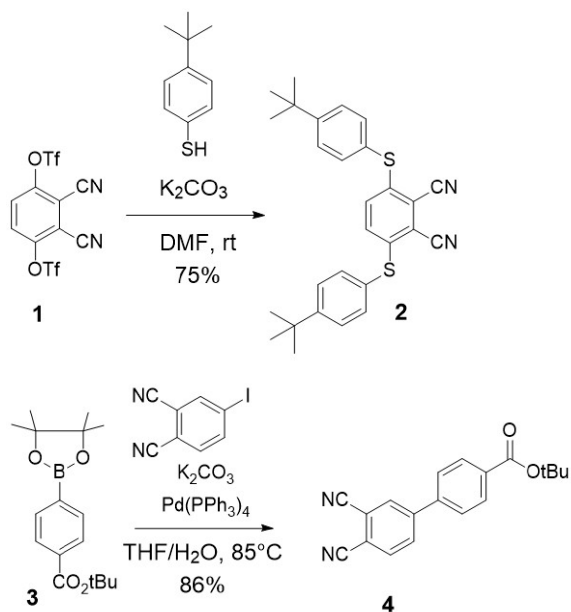
Finding sustainable and environmentally friendly strategies to generate energy represents a huge challenge for modern society because of the inevitable depletion of widely used fossil fuels and the pollution they generate. Solar energy, and more specifically photovoltaic (PV), appears like a perfect alternative to non-sustainable fossil fuels [1]. An original approach, consisting in developing transparent and colorless solar panels, represents a “disruptive technology” because it opens new applications. For examples, transparent solar cells would be suitable for integration in Building-Integrated Photovoltaics (BIPV) [2] such as in windows of buildings, but also for electric vehicles, and self-powered greenhouses [3–5]. However, the integration of PV into building windows require a visible light transmittance higher than 55% for good visual perception [6] and the absence of color is necessary in order to provide good aesthetics.

Over the years, the development of Transparent PhotoVoltaics (TPV) has grown considerably [7]. However, such devices are mainly absorbing visible light and the transparency is mostly modulated by the thickness of the active layer or by the introduction of microscopic holes in the film [8]. Another approach consists in the transmission of light in the visible region through selective absorption of UV (<380 nm) and NIR (>700 nm) light. Some inorganic [9] and organic [10] systems were investigated but although very high Average Visible Transmittance (AVT) [11] values were achieved, the technology requires further improvement to increase the final efficiency.

Mainly popularized by O'Regan and Grätzel in 1991 [12], Dye-Sensitized Solar Cells (DSSCs) represent a relevant candidate for highly transparent and neutral-colored photovoltaic devices. First, they are potentially cheap to produce. Second, their efficiencies are less dependent on the light incidence angle and intensity, and particularly they outperform classical inorganic-based cells under diffuse irradiance [13,14]. Third, the device is based on a thin layer of TiO₂ nanoparticles sensitized by light-harvesting dyes, meaning that DSSCs can virtually absorb within any desired spectral region, depending mainly only on the selected dye [15]. Historically, dyes employed on DSSCs are based on

Ru(II)-polypyridyl complexes [16], zinc porphyrins [17], or even metal-free organic dyes [18,19] reaching an efficiency higher than 14% [20], but all these dyes absorb in the visible range and the corresponding DSSCs exhibit an intense coloration. On the other hand, using dyes which absorb only NIR radiations is a tantalizing option to prepare efficient, transparent and colorless DSSCs, given the high photon flux of the solar spectra in the 700–1000 nm range. Finally, in DSSC, both the photoanode and the counter electrode can be transparent allowing illumination from both sides and are therefore compatible with see-through photovoltaics.

The first example of transparent DSSC for see-through photovoltaic windows was reported by Zhang *et al.* in 2014 and presents the combination of UV and NIR dyes that reach a final power conversion efficiency (PCE) of 3.66% with an AVT higher than 60% [21]. Very recently Sauvage and co-workers [22], reported a transparent DSSC with a cyanine dye (coded VG20) which exhibits a PCE of 3.1% with an impressive AVT of 76%. Among the NIR absorbing dyes in DSSC, such as cyanines [23–25] and squaraines [26–28], phthalocyanine derivatives represent suitable candidates due to an intense absorption close to NIR region of the solar spectrum, a high molar extinction coefficient and a high fluorescence quantum yield, a great stability and proved efficiency in DSSCs [29]. This is especially true since the seminal work of Ikeuchi *et al.* when highly bulky groups were tethered to the macrocycle in order to limit deleterious aggregation, leading to a very significant jump in the photoconversion efficiencies, reaching 6% [30]. Phthalocyanines are highly stable tetrapyrrolic macroheterocycles constituted by four isoindole units. Their properties can be easily tuned by the nature of the substituent linked to the macrocycle unit and by the atom or ion coordinated in the macrocycle. However, most phthalocyanine derivatives present an intense Q band centered around 650–700 nm [31]. In order to shift this transition further into the NIR, grafting electron-rich substituents in the α -positions of the Pc macrocycle has proven to be a successful strategy. Indeed, the addition of S-Aryl unit in α -positions induce a significant redshift of the absorption band (of about 80 nm) compared to previous Pcs substituted in β -position with O-Aryls substituent [32,33]. It thus appears relevant to graft



Scheme 1. Synthesis of phthalonitrile **2** and **4**.

very bulky groups *via* a thioether linkage on the Pc macrocycle in order to both redshift the absorption and prevent dye aggregation on TiO₂'s surface to some extent [34].

In this report, we have designed and synthesized a new phthalocyanine derivative **KMH63** containing six thiophenyl-tert-butyl units in α -positions of the macrocyclic and one carboxylic acid as anchoring group directly connected to the core by a phenyl spacer (Scheme 2). Our main finding is that **KMH63** displays adequate optical and electrochemical properties to design colorless transparent photoelectrodes. However, the performances of the DSSC remain weak because of a weak electron injection driving force that can be solved by changing the spacer linking the anchoring group and the phthalocyanine unit.

2. Synthesis

The synthesis of **KMH63** requires the two key phthalonitriles **2** [35] and **4** [36] as reagents (Scheme 1). 3,6-bis(thiophenyl-tert-butyl)phthalonitrile **2** was prepared in 75% yield by nucleophilic aromatic substitution of phthalonitrile-3,6-ditriflate **1** by 4-tertbutylthiophenol [37].

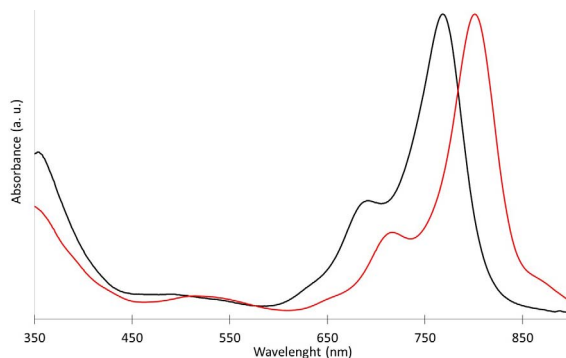


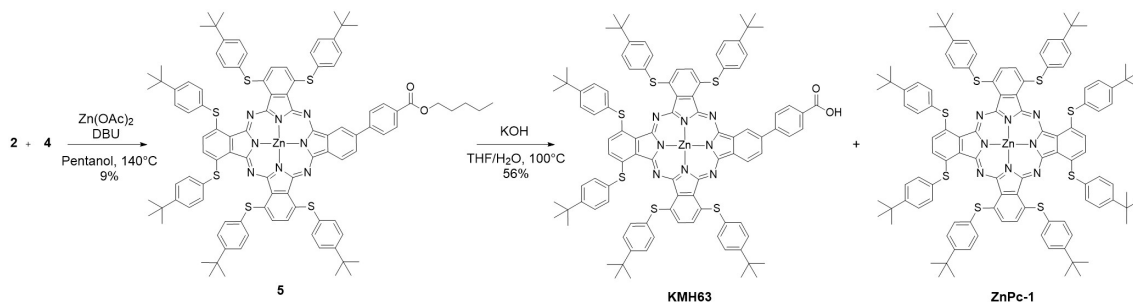
Figure 1. Normalized absorption of **KMH63** (black) and **Zn-Pc-1** (red) recorded in dichloromethane solution.

The second phthalonitrile **4** was synthesized according to a Suzuki–Miyaura cross-coupling reaction between the boronic ester **3** [38] with iodophthalonitrile with a good yield of 86%. Following the conditions described by Giribabu *et al.* [39], using zinc(II) as template and 1,8-diazabicyclo[5.4.0]undec-7-ene (DBU) as a base, the cross-condensation of both phthalonitrile derivatives **2** and **4** in pentanol afforded the ester-protected phthalocyanine **5** in 9% yield after purification by preparative thin layer chromatography (Scheme 2). ¹H NMR spectrum and mass spectrometry analysis revealed that the tert-butyl ester was transesterified by pentanol during this reaction. However, this side reaction does not have any consequence since the pentyl ester was saponified by potassium hydroxide to lead to the desired product **KMH63** in 56% yield (Scheme 2).

3. Electronic absorption and emission properties

The absorption and emission spectra of **KMH63** were recorded in dichloromethane solution at room temperature (Figures 1 and S5). The optical data including wavelengths of maximal absorption (λ_{abs}), extinction coefficients (ϵ), wavelength of maximal emission (λ_{em}) and zero-zero energy level of the lowest singlet excited state (E_{00}), are collected in Table 1.

The absorption spectrum of **KMH63** displays the usual spectral signatures of zinc phthalocyanine derivatives [31]. It is dominated by an intense and thin Q band, corresponding to π – π transitions, at 768 nm and a lower intensity Soret band at 358 nm.



Scheme 2. Synthesis of zinc phthalocyanine **KMH63**.

Table 1. Wavelength of maximal absorption (λ_{abs}) with extinction coefficient (ϵ), wavelength of maximal emission (λ_{em}) recorded at room temperature in dichloromethane and zero-zero energy level of the lowest excited state (E_{00})

Dye	$\lambda_{\text{abs}}/\text{nm}$ ($\epsilon \times 10^{-3}/\text{M}^{-1} \cdot \text{cm}^{-1}$)	$\lambda_{\text{em}}/\text{nm}$	E_{00}/eV
KMH63	358 (40800); 696 (28700); 768 (75500)	787	1.59

Weaker Q band at 696 nm is also observed and can be attributed to vibronic overtone [40]. As expected, the presence of six S-Aryl units in α -position of the macrocyclic system allows a significant redshift of the absorption band compared to classical unsubstituted or O-Aryls substituted zinc phthalocyanines. Importantly, there is a large wavelength region where the phthalocyanine derivative does not absorb (between 450 and 600 nm), which is favorable to provide transparency in the visible region. Interestingly, the spectrum of the parent octa α -substituted S-Aryles zinc phthalocyanine is even more shifted to the red region [33], with maximum absorption wavelength around 800 nm, underscoring that the removal of only two aryl thioether units on the phthalocyanine has a significant effect on the electronic properties (Figure 1).

KMH63 is a fluorescent dye with an emission maximum wavelength located at 787 nm enabling us to calculate the E_{00} , which was estimated to 1.59 eV (Figure S5 and Table 1).

Then, the absorption spectrum of the phthalocyanine **KMH63** was recorded on thin TiO_2 film with several concentrations of chenodeoxycholic acid (CDCA) in the dyeing bath (Figures 2 and S1). On TiO_2 surface, the dye clearly exhibits a significant broadening and a hypsochromic shift of the Q band, which is assigned to the formation of H-type

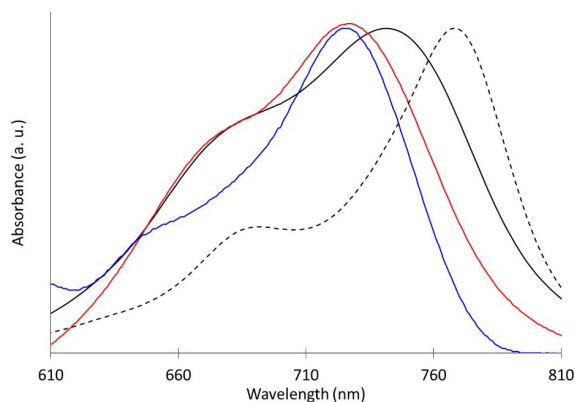


Figure 2. Normalized absorption spectra of **KMH63** on 2 μm thick TiO_2 nanocrystalline film 0 mM (black), 5 mM (red) and 20 mM (blue) of CDCA along that in solution (black dotted line).

aggregates. In order to support this hypothesis, controlled amounts of anti-aggregate CDCA were added during the chemisorption step. Indeed, the presence of CDCA (20 mM) reduces the intensity of the shoulder at 675 nm band and of the bathochromic shift indicating a diminution of the aggregation process. Lower quantities of CDCA (5 mM) proved to be less efficient to overcome this problem.

Table 2. Redox potentials recorded by cyclic voltammetry at room temperature in dimethylformamide solution with Bu₄NPF₆ (0.1 M) as supported electrolyte and referenced versus saturated calomel electrode (SCE)

Dye	$E(S^+/S)$ V <i>vs.</i> SCE	$E(S/S^-)$ V <i>vs.</i> SCE	$E(S^+/S^*)$ V <i>vs.</i> SCE	$\Delta G_{\text{inj}}^\circ$ (eV)	$\Delta G_{\text{reg}}^\circ$ (eV)
KMH63	0.63	−0.77	−0.96	−0.26	−0.43

Calculated Gibbs free energies for electron injection ($\Delta G_{\text{inj}}^\circ$) and dye regeneration ($\Delta G_{\text{reg}}^\circ$).

4. Electrochemical properties

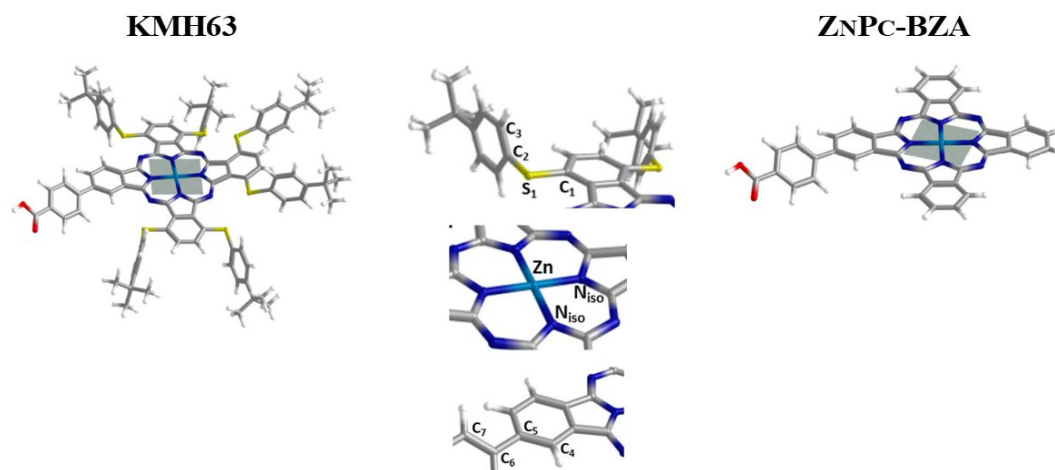
The new phthalocyanine **KMH63** was studied by cyclic voltammetry to determine its redox potentials and to calculate the hole injection ($\Delta G_{\text{inj}}^\circ$) and dye regeneration ($\Delta G_{\text{reg}}^\circ$) driving forces (Table 2). The cyclic voltammogram of **KMH63** is shown in Figure S4. **KMH63** exhibits a reversible one-electron oxidation wave at 0.63 V *vs.* SCE, corresponding to the formation of the radical cation on the phthalocyanine macrocycle. A reversible reduction wave is observed at −0.77 V, followed by an irreversible one at −1.17 V *vs.* SCE. The calculated oxidative potential of the singlet excited state of **KMH63** is not as negative (−0.96 V *vs.* SCE) as previously reported β -S-Ar or β -O-Ar-substituted zinc phthalocyanines [41], resulting in a moderate, though suitable $\Delta G_{\text{inj}}^\circ$. On the one hand, the oxidation potential of **KMH63** is much higher than that of the redox potential of I^-/I_3^- (0.2 V *vs.* SCE) thus affording a calculated $\Delta G_{\text{reg}}^\circ$ value around −0.4 eV, suggesting a significant dye regeneration driving force with iodide. On the other hand, the injection driving force is significant to expect a good injection quantum yield, particularly if the electrolyte contains lithium cation to bend downward the conduction band.

5. Computational study

The UV–Vis absorption spectrum for **KMH63** was calculated in the solution phase using the optimized molecular geometry employing the time-dependent density functional theory (TDDFT) approach [42–46] at the M06/6-31G(d,p) level of theory. More details about the optimization method used are included in the supporting information. This functional (M06) [47] has been used by us in previous works with excellent results [48–50]. The electronic excitations were modeled as singlet–singlet vertical

transitions of the Franck–Condon type. We computed 30 excited states to cover the region of both the Q and B bands. We choose dichloromethane (CH₂Cl₂) as the solvent because the UV–Vis spectrum of **KMH63** was measured in that solvent. The solvent was simulated with the Conductor-like Polarizable Continuum Model (CPCM) [51,52] and a dielectric constant of 8.93. To understand the absorption bands, isosurfaces for the molecular orbitals (MOs) involved in the electronic transitions were built up, i.e. the highest occupied (HOMOs) and lowest unoccupied (LUMOs) MOs. In cases where the excited state is formed from several electronic transitions, we have preferred to calculate the natural transition orbitals (NTO) [53]. These ones have the advantage that all the transitions are considered and an account of the whole excited state is given. In order to get a better comprehension about the electronic absorption properties of **KMH63**, we compared our theoretical results with the absorption spectrum of Zn(II) phthalocyanine, where we have maintained the benzoic acid (BZA) in the β -position as in **KMH63**, because it is the moiety that interacts with the semiconductor (TiO₂). This system was coded **ZnPc-BZA** (Scheme 3). All the calculations related to the molecular geometry optimization, electronic absorption spectra and molecular orbitals were performed with the package Gaussian 09, rev.D.01 [54].

To determine the interaction between the dye and the semiconductor (TiO₂), systems were computed after grafting the dye on a TiO₂ anatase cluster model. This model was prepared from the anatase-phase (101) crystallographic structure and corresponds to a surface consisting of 40 titanium atoms, 82 oxygen atoms and four hydrogen atoms [Ti₄₀, O₈₂, H₄] saturating the oxygen dangling bonds. The geometry of the complex is partially optimized, where TiO₂ is frozen to retain the anatase-phase structure, and the dye with the anchoring group (−COOH)



Scheme 3. Optimized molecular structures of **KMH63** and **ZnPc-BZA** where the plane formed by Zn(II) and the four N atoms of the macrocycle is shown.

approaching to a titanium atom are fully optimized. The interaction between the fragments is monodentate meaning that one -O(OH) interacts with one titanium atom. The complex was optimized at the DFT level of theory with the D3 Grimme's dispersion correction using the Quantum ATK package [55]. All of the atoms were represented by a double- ζ -polarized (DZP) basis set, along with the PseudoDojo norm-conserving pseudopotential, employing the Perdew–Burke–Ernzerhof (GGA-PBE) [56,57] exchange-correlation functional. The interaction energy was calculated by using the following formula $\Delta E_{\text{int}} = E_{\text{dye-TiO}_2} - (E_{\text{TiO}_2} + E_{\text{dye}})$ and the fragments dye and TiO_2 were used with the optimized geometry obtained in the complex. The correction of the ΔE_{int} for the basis set superposition error was not calculated because of the size of the system dye- TiO_2 .

On the other hand, aromaticity has been assessed using three different criteria: the magnetic one [58] via the gauge independent atomic orbital (GIAO) method [59]. The module of magnetically induced current density [60] (MICD) have been plotted 1.0 a.u. above the molecular plane obtained by means of Quantum Theory of Atoms in Molecules (QTAIM) [61]. In addition, the popular nucleus independent chemical shift (NICS) and its z -component [62] (NICS_{zz}) have been measured in strategic positions, these indexes are especially reliable for π -aromaticity analysis [62–65] and allows quantifying the magnetic response due to ring

currents. These calculations were performed using Gaussian 09 in conjunction with AIMAll software [66] and MICD module planes were plotted using VisIt software [67].

Additionally, the delocalization criteria [68] have been applied using the recently proposed AV1245 index [69], specially designed for macrocycles such as porphyrinoids, whereas the multi-center index [70] (MCI) and para-delocalization index [71] (PDI) have been used to analyze the six-membered rings (6MR). Finally, the geometric criteria has been evaluated using the Harmonic Oscillator Model of Aromaticity [72] (HOMA), these indexes were calculated using the Multiwfn program [73].

The optimization of the ground-state geometries of **KMH63** and **ZnPc-BZA**, in general, successfully reproduced the geometrical parameters of these compounds. In both dyes, the average bond lengths between Zn (II) ions and the four isoindole nitrogen atoms are 1.991 Å. A good correlation was obtained for the Zn–N calculated bond lengths with other phthalocyanines reported, such as Zn(II) phthalocyanine and Zn(II)octa- β -methoxyphthalocyanine, whose average Zn–N bond lengths are 2.010 Å and 2.011 Å, respectively, computed at the BP86/def2-SVP+D3BJ level of theory [74]. Others studies also include reported theoretical values of the mean bond distances Zn–N of 2.012 Å for a family of dimers di-Zn(II)-pyrazinoporphyrazine-phthalocyanine complexes with different peripheral substituents (R), cal-

Table 3. Singlet→Singlet absorption vertical transitions computed at the M06/6-31G(d,p) theoretical level considering the solvent effect via conductor polarizable continuum model (CPCM)/dichloromethane

System	E_{HL}	E	λ	f	Band	Assignment	Main MOs
KMH63	2.11	1.64	756	0.80	Q	$\pi(\text{pht}) \rightarrow \pi^*(\text{pht})$	H → L
		1.66	748	0.88	Q	$\pi(\text{pht}) \rightarrow \pi^*(\text{pht})$	H → L + 1
		3.30	375	0.17	B	$\pi(\text{pht}) \rightarrow \pi^*(\text{pht})$	NTO 14 occ → virt
ZnPc-BZA	2.35	1.89	655	0.77	Q	$\pi(\text{pht}) \rightarrow \pi^*(\text{pht})$	H → L
		1.93	641	0.62	Q	$\pi(\text{pht}) \rightarrow \pi^*(\text{pht})$	H → L + 1
		3.80	327	0.58	B	$\pi(\text{pht}) \rightarrow \pi^*(\text{pht})$	NTO 19 occ → virt

Excitation wavelength (λ/nm), energy (E/eV), oscillator strength (f) and the corresponding molecular orbitals (MOs) involved in the electronic transitions, as also the band assignment. The HOMO–LUMO energy difference (E_{HL}/eV) is also included.

culated at the BP86/Slater-type orbital (STO) basis sets with triple- ζ accuracy plus polarization function (TZP) theoretical level [75].

The presence of tert-Butylbenzenethiol groups in **KMH63** clearly produces an out-of-the-plane deviation of the isoindole moieties by 2°–3°, compared to **ZnPc-BZA** where the macrocycle structure is completely planar. In compound **KMH63**, the optimized conformation displays the phenyl ring of the tert-Butylbenzenethiol substituents perpendicularly to the macrocycle, with average dihedral angles $\angle C_1 - S_1 - C_2 - C_3$ between the phenyl rings of substituent in the α -position from 88.7° to 91.5°. In **KMH63** and **ZnPc-BZA**, the average bond angle formed between isoindole N atoms and Zn (II) ion ($\angle \text{Niso} - \text{Zn} - \text{Niso}$) is 90°. The dihedral angle $\angle C_4 - C_5 - C_6 - C_7$ formed by isoindole units and benzyl ring of the benzoic acid (anchor group) in the β -position does not show significant differences, which is 143.89° and 143.27° for **KMH63** and **ZnPc-BZA**, respectively. The optimized structures for these compounds do not indicate a displacement of Zn(II) ion from the molecular plane defined by the four isoindole N atoms (Scheme 3).

The electronic absorption spectrum of **KMH63** has been simulated using the time-dependent DFT (TDDFT) approach in the solution phase and the analysis of the resulting parameters; excitation wavelength (energy), the oscillator strength and the electronic transitions between MOs, were performed (Table 3). To investigate the effect of the tert-Butylbenzenethiol substituents in the α -positions in the phthalocyanine, we have compared the spec-

troscopic results of **KMH63** with the substituent-free macrocycle (**ZnPc-BZA**) (Scheme 3).

Table 3 shows that both compounds (**KMH63**, **ZnPc-BZA**) present two strong Q bands and one B band of lower intensity, as expected for phthalocyanines, but the presence of the substituents in **KMH63** increases much more the difference in the intensity of the Q and B bands, 0.80(0.88) against 0.17, respectively. Another notorious effect is the redshifting of the two Q bands from **ZnPc-BZA** to **KMH63** by 101 and 107 nm, respectively, and for the B bands in 48 nm. It means that one form to achieve an important absorption near to infrared is to use these kinds of substituents, where the tert-butyl and the benzenethiol are electron donor moieties that inject electron density to the macrocycle. This behavior of the substituents can be seen in the electrostatic potential calculated for the ground state, as shown in Figure 3. The system **ZnPc-BZA** presents four blue regions localized on the aza nitrogen atoms that represent negative regions and charge concentration, as the color scale indicates. The blue region is widely increased along the macrocycle core in **KMH63** indicating a larger charge concentration available to be excited to higher energy levels (LUMOs).

The theoretical value for the Q band of longest wavelength in **KMH63** is well compared with the experimental value measured in this work of 768 nm (1.61 eV), with a very small deviation of 0.03 eV. This confirms that the theoretical method used (M06/6-31G(d,p)) for the simulation of the spectrum has been adequate.

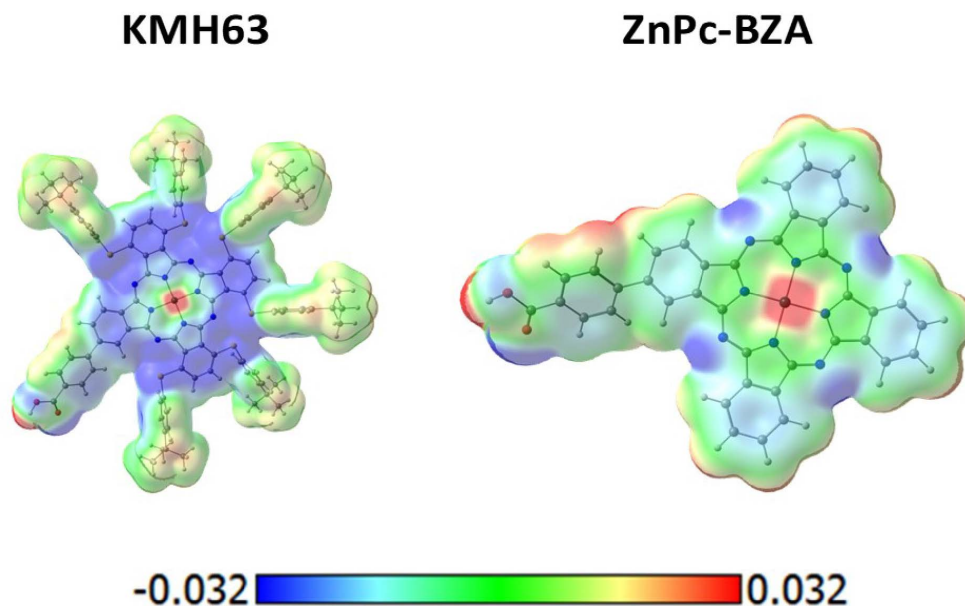


Figure 3. Molecular electrostatic potential calculated at the M06/6-31G(d,p) level of theory in dichloromethane. The color scale is added at the bottom.

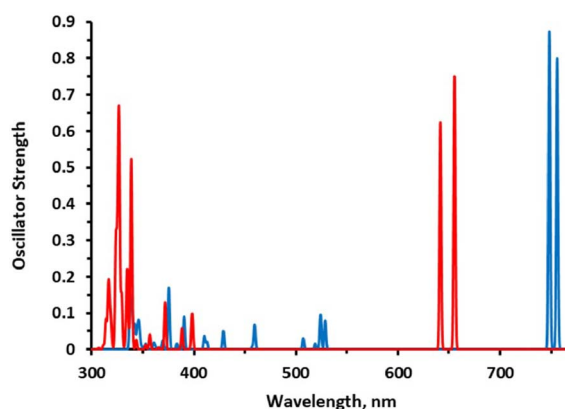
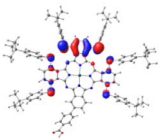
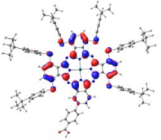
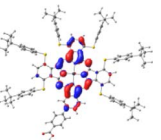
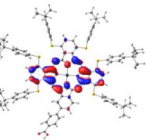
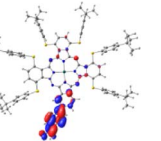
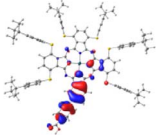
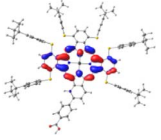





Figure 4. Electronic absorption spectra calculated at the M06/6-31G(d,p) level of theory in dichloromethane; **KMH63** blue and **ZnPc-BZA** red.

Figure 4 shows a comparison of the spectra of **KMH63** and **ZnPc-BZA**, and clearly Q higher and pronounced bands can be seen as also an important bathochromic shifting for the former. For **KMH63** a wider absorption is observed in the B region in about 350–550 nm, but in contrast to the case of **ZnPc-BZA** the absorption is concentrated in a shorter region (300–400 nm), but the bands with a higher intensity near to 300 nm.

Table 4 shows the frontier MOs from HOMO–1 to LUMO+2 to understand the absorption bands calculated as mentioned above. In both systems, the excited states belonging to the two Q bands correspond to the electronic transitions $H \rightarrow L$ and $H \rightarrow L+1$. In both cases, the orbitals are centered mainly on the phthalocyanine macrocycle and there is neither the participation of the substituents nor of the anchor group. These results suggest that the electron

Table 4. Surfaces of the frontier MOs with their energies (eV), and the natural transition orbitals (NTO) calculated at the M06/6-31G(d,p) level of theory in dichloromethane

System	HOMO-1	HOMO	LUMO	LUMO+1	LUMO+2
KMH63					
	-5.886	-4.992	-2.882	-2.859	-1.589
	NTO14 occ	NTO 14 virt			
ZnPc-BZA					
	-6.794	-5.228	-2.880	-2.843	-1.585
	NTO19 occ	NTO 19 virt			

injection process from the virtual orbitals (L, L+1) of **KMH63** or **ZnPc-BZA** to the conduction band of the semiconductor (TiO_2) would not be favorable. Zhang and co-workers [76,77] reported that heteroatom-metal interaction in metal phthalocyanines, such as S-Zn, is possible. For this reason, the optimization of J and H dimers (Figure S6) was performed at the B3LYP/6-31G(d,p) level of theory. However, distances of 4.98 Å and 6.67 Å, respectively were found. These distances are much larger than those reported for the Zn-S interaction (2.3 Å–2.6 Å), which evidences the absence of metal-sulfur interactions. This interaction is avoided due to the presence of bulky substituents, which prevents the formation of such aggregates.

However, the theoretical results indicate that the electron injection could occur from L+2 to the semiconductor because it is completely centered on the benzoic acid, but it would require an energy of

3.4 eV (365 nm), very high (UV region) to be an attractive compound to be used in DSSCs. On the other hand, the B bands of **KMH63** and **ZnPc-BZA** that correspond to the excited state 14 and 19, respectively, were analyzed with the natural transition orbitals (NTO). These correspond to transitions between NTOs centered on the macrocycle, as expected for these kinds of bands. All the bands correspond to $\pi \rightarrow \pi^*$ electronic transitions.

In summary, the compound **KMH63** has the advantage over **ZnPc-BZA** in that it presents redshifted absorption and more intense Q bands, although this characteristic is not enough to be a good photosensitizer for DSSCs. The electron injection would not be favorable in the visible light region, as shown by the molecular orbitals.

Finally, the interaction of **KMH63** and **ZnPc-BZA** with a TiO_2 anatase model was simulated. The optimized molecular structures shown in Figure 5

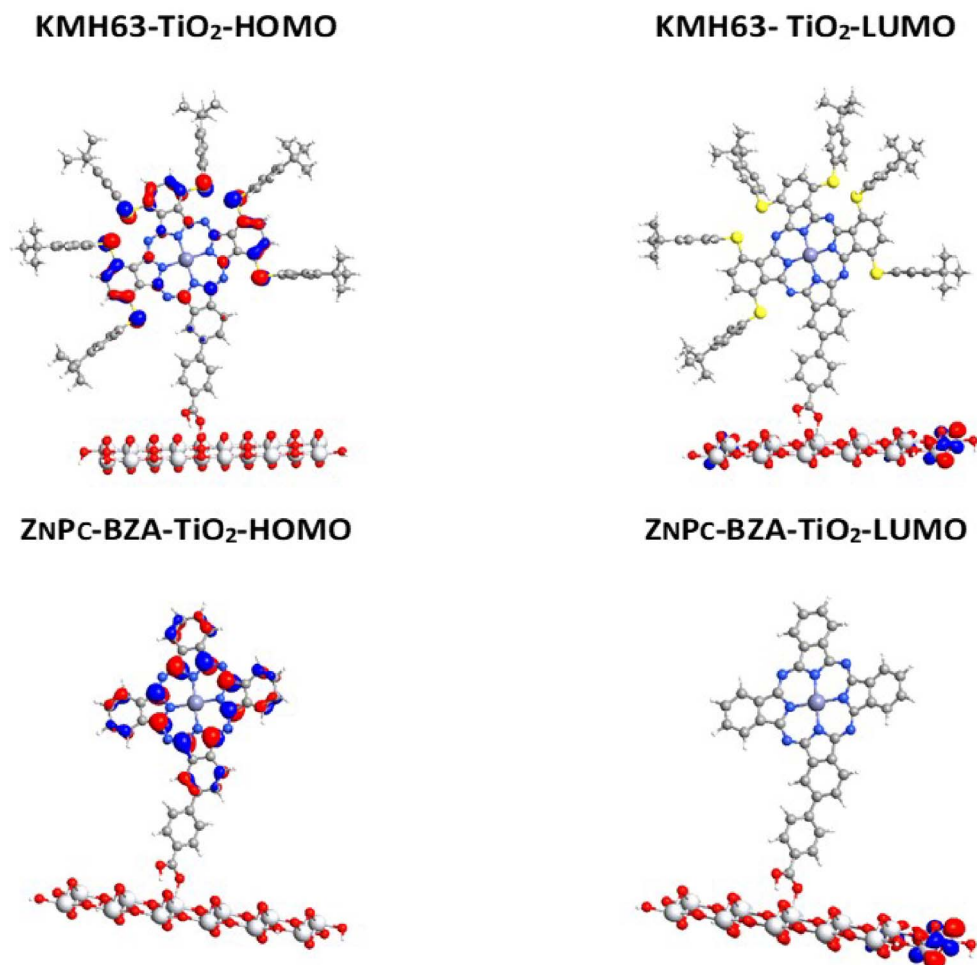


Figure 5. Frontier molecular orbitals for the complexes **KMH63**-TiO₂ and **ZnPc-BZA**-TiO₂. Color coding: silver = titanium, red = oxygen, blue = nitrogen, light blue = zinc, gray = carbon, white = hydrogen.

indicate an approaching of the oxygen atom of the carbonyl group ($-\text{O}(\text{C}=\text{O})$) toward one titanium atom with a distance of 2.10 Å in both **KMH63** and **ZnPc-BZA**. The finding is in agreement (2.26 Å) with the adsorption of acetic acid on a surface model of TiO₂ anatase (101) calculated by Manzhos *et al.* [78] using the self-consistent charge density functional tight binding scheme (SCC-DFTB) for a monodentate interaction mode. Furthermore, the hydrogen atom of the hydroxyl group ($-\text{O}(\text{OH})$) shows the formation of a hydrogen bonding with an oxygen atom of TiO₂ cluster with a distance of 1.30 Å for both **KMH63** and **ZnPc-BZA**, which is comparable to the distance calculated by Manzhos *et al.* [78] of 1.62 Å. Our results indicate that the interaction distance

would not be affected by the substituent groups but also confirm that a favorable interaction is given between the $-\text{COOH}$ moiety and both the titanium and oxygen atoms of TiO₂.

We also calculated the interaction energy (E_{int}) and found that both phthalocyanines present a negative value that indicates a favorable interaction between the fragments (**KMH63**/**ZnPc-BZA** and TiO₂). The complex **KMH63**-TiO₂ (−2.6 eV) shows a larger interaction of 0.2 eV (4.6 kcal/mol) than the complex **ZnPc-BZA**-TiO₂ (−2.4 eV), although the difference of E_{int} could be considered small. Moreover, the calculations indicate that the three tert-Butylbenzenethiol substituents do not hinder the binding of the phthalocyanine on TiO₂ surface.

Table 5. Photovoltaic parameters for DSSCs sensitized with **KMH63** dye measured under simulated AM 1.5G, 1 Sun illumination

Cell	Additives	TBP	J_{sc} (mA/cm ²)	V_{oc} (mV)	FF (%)	PCE (%)
1	no CDCA	0 M	0.84 ± 0.14	442 ± 2	68 ± 1	0.26 ± 0.04
2	20 mM CDCA	0 M	1.23 ± 0.32	461 ± 7	72 ± 2	0.41 ± 0.12
3	20 mM CDCA	0.2 M	0.47 ± 0.01	559 ± 1	71 ± 2	0.19 ± 0.01

Additionally, we calculated the frontier molecular orbitals of both complexes to confirm their donor-acceptor nature. Figure 5 shows that in both, the donor species is the phthalocyanine because the HOMO is located there, and the acceptor species is the TiO₂ because the LUMO is located on this fragment. However, the HOMO surface of **KMH63** displays that the higher energy electrons are centered in the benzene rings and on the sulfur atoms. In contrast, HOMO surface of **ZnPc-BZA** is concentrated on the pyrrole and the benzene rings. Furthermore, the gap HOMO-LUMO of **KMH63**-TiO₂ (0.39 eV) is lower than that of **ZnPc-BZA**-TiO₂ (0.69 eV), which suggests a more reactive complex in the former and could be of benefit for the charge transfer to the semiconductor TiO₂.

The analysis of the aromaticity reveals a strong diatropic ring current in the main rings of **KMH63** and **ZnPc-BZA**. In addition, the benzenoid rings (6MR) of **KMH63** present a significant reduction in aromaticity due to the substituent effect when compared to **ZnPc-BZA**. Computed indexes show that there is a notable difference in the magnetic response, degree of delocalization, bonding distance and conjugation of the macrocycle. The internal cross of the macrocycle in **KMH63** is less aromatic than **ZnPc-BZA**, as well as the 6MRs, except for those attached to the carboxyl group (See Figure S7 in the SI), which is the most aromatic because it is not affected by the thiophenyl-tert-butyl units and shows similar values for both compounds. Further details can be found in the supporting information.

6. Photovoltaic characterizations

Dye-sensitized solar cells were assembled using **KMH63** as sensitizer on mesoporous TiO₂ as working electrode, platinized conducting glass as the counter electrode and iodide/triiodide in acetonitrile as electrolyte (see experimental part for details). The

photovoltaic performances of solar cells recorded under AM 1.5 are summarized in Table 5 and the current-voltage characteristics are given in supporting information material (Figure S3). The first measurements were performed with two different ratios of CDCA (0 mM and 20 mM) and using an electrolyte without tert-butyl-pyridine (TBP) (composition: 50 mM I₂, 0.1 M LiI, 0.6 M Li in acetonitrile). In the absence of CDCA, the overall performances are lower than those with 20 mM of CDCA, passing from 0.26% to 0.41% power conversion efficiencies (PCEs) owing to weaker J_{sc} , V_{oc} and even FF. This result can be reasonably explained by a diminution of the H-aggregates in the presence of CDCA that certainly quenches the excited state and diminishes electron injection efficiency. Overall, the PCE of this new dye **KMH63** is quite low compared to previous phthalocyanines reported in the literature, which presents very good efficiency around 6% and even higher [16]. In a second step, the addition of TBP in the electrolyte was investigated. TBP is known to adsorb on TiO₂ surface to prevent interfacial charge recombination with the electrolyte and to induce an upward conduction band bending, which enables enhancing of the V_{oc} [79,80]. With TBP, the DSSC exhibits a significant drop of the photocurrent density (from 1.23 to 0.47 mA/cm²), reflecting a lower electron injection quantum yield that might be due to a sluggish injection reaction owing to a decrease of the driving force resulting in a more negative TiO₂ conduction band. This result confirms that the electron injection from the dye to TiO₂ is one the main limiting factors of **KMH63**. Even if the low ΔG_{inj}° is thermodynamically favorable and theoretically permits an efficient electron injection, the driving force and the electronic coupling are certainly too low to guarantee efficient injection. This is consistent with computational studies that show that the spin density of the LUMO orbital in **KMH63**, is poorly distributed on the anchoring group, thus limiting the

electronic communication with the TiO₂ conduction band. In a recent publication, Torres and co-workers reported a very bulky zinc phthalocyanine sensitizer exhibiting similar low PCE as **KMH63** [81]. It was proposed that the low dye loading of this bulky phthalocyanine was at the origin of weak light capture, restricting its light-harvesting efficiency. Although this possibility cannot be fully excluded here, this study shows that upon addition of CDCA in the dye bath, the photoconversion of the solar cell is raised (Table 2), while the dye loading is necessarily decreased as confirmed by the lower coloration of the TiO₂ film (Figure S1). Accordingly, we can conclude that the dye loading of **KMH63** is certainly not the main reason for the low efficiency of this dye.

7. Conclusion

In this study, a new zinc phthalocyanine sensitizer was prepared to explore the possibility of making transparent and colorless DSSCs. The absorption and photoelectrochemical properties indicate that this compound fulfills the criteria for such application. Detailed computational calculations enable a deeper understanding of the electronic properties of this sensitizer and particularly that the presence of bulky thio-aryl substituents does not hinder the approach of the dye on the surface and do not perturb its chemisorption on TiO₂ surface. On the other hand, it was shown that the electronic communication of **KMH63** with TiO₂ conduction is weak owing to the absence of overlapping of LUMO and LUMO+1 with the semiconductor wavefunction, precluding a sluggish electron injection. The modest photovoltaic performances measured in TiO₂-based DSSC are certainly due to inefficient electron injection and could be certainly enhanced with a different spacer connecting the phthalocyanine to the anchoring group. For example, the utilization of a more π -conjugated system such as acrylic acid or cyano-acrylic acid would be more favorable to assist electron injection. We are working towards this goal and the results will be communicated in due course.

Acknowledgments

We acknowledge financial support by Agence Nationale de la Recherche (ANR) through the program Vision-NIR (ANR-17-CE05-0037-02) Région des Pays

de la Loire for the project LUMOMAT and ECOS Sud-CONICYT (Chili). We thank the financial support of ANID/CHILE under the following projects: FONDECYT 1171719 (GC-J) and 1180565 (XZ), FONDECYT Postdoctoral 3180119 (RP-R) and ECOS C19E03 (GC-J, XZ). MZ-A is grateful for the graduate fellowship awarded by the Vicerrectoría de Postgrado (VIPO) of USACH/CHILE, and YH-R is grateful for the PhD Program in Molecular Physical Chemistry from University Andres Bello/CHILE. Powered@NLHPC: This research was partially supported by the supercomputing infrastructure of the NLHPC (ECM-02) of the Universidad de Chile.

Supplementary data

Supporting information for this article is available on the journal's website under <https://doi.org/10.5802/crchim.113> or from the author.

References

- [1] V. V. Tyagi, N. A. A. Rahim, N. A. Rahim, J. A. L. Selvaraj, *Renew. Sustain. Energy Rev.*, 2013, **20**, 443-461.
- [2] B. Joseph, T. Pogrebnaya, B. Kichonge, *Int. J. Photoenergy*, 2019, article no. 5214150.
- [3] E. Ravishankar, M. Charles, Y. Xiong, R. Henry, J. Swift, J. Rech, J. Calero, S. Cho, R. E. Booth, T. Kim, A. H. Balzer, Y. Qin, C. Hoi Yi Ho, F. So, N. Stingelin, A. Amassian, C. Saravitz, W. You, H. Ade, H. Sederoff, B. T. O'Connor, *Cell Rep. Phys. Sci.*, 2021, **2**, article no. 100381.
- [4] A. Dessì, D. A. Chalkias, S. Bilancia, A. Sinicropi, M. Calamante, A. Mordini, A. Karavioti, E. Stathatos, L. Zani, G. Reginato, *Sustain. Energy Fuels*, 2021, **5**, 1171-1183.
- [5] G. P. Kini, S. J. Jeon, D. K. Moon, *Adv. Funct. Mater.*, 2021, **31**, article no. 2007931.
- [6] C. Tuchinda, S. Srivannaboon, H. W. Lim, *J. Am. Acad. Dermatol.*, 2006, **54**, 845-854.
- [7] K. Lee, H.-D. Um, D. Choi, J. Park, N. Kim, H. Kim, K. Seo, *Cell Rep. Phys. Sci.*, 2020, **1**, article no. 100143.
- [8] A. Takeoka, S. Kouzuma, H. Tanaka, H. Inoue, K. Murata, M. Morizane, N. Nakamura, H. Nishiwaki, M. Ohnishi, S. Nakano, Y. Kuwano, *Sol. Energy Mater. Sol. Cells*, 1993, **29**, 243-252.
- [9] Y. Zhao, R. R. Lunt, *Adv. Energy Mater.*, 2013, **3**, 1143-1148.
- [10] R. R. Lunt, V. Bulovic, *Appl. Phys. Lett.*, 2011, **98**, article no. 113305.
- [11] C. Yang, D. Liu, M. Bates, M. C. Barr, R. R. Lunt, *Joule*, 2019, **3**, 1803-1809.
- [12] B. O'Regan, M. Grätzel, *Nature*, 1991, **353**, 737-740.
- [13] M. Freitag, J. Teuscher, Y. Saygili, X. Zhang, F. Giordano, P. Liska, J. Hua, S. M. Zakeeruddin, J.-E. Moser, M. Grätzel, A. Hagfeldt, *Nat. Photonics*, 2017, **11**, 372-378.
- [14] D. Zhang, M. Stojanovic, Y. Ren, Y. Cao, F. T. Eickemeyer, E. Socie, N. Vlachopoulos, J.-E. Moser, S. M. Zakeeruddin,

- A. Hagfeldt, M. Grätzel, *Nat. Commun.*, 2021, **12**, article no. 1777.
- [15] M. Godfroy, J. Liotier, V. M. Mwalukuku, D. Joly, Q. Huaulmé, L. Cabau, C. Aumaitre, Y. Kervella, S. Narbey, F. Oswald, E. Palomares, C. A. G. Flores, G. Oskam, R. Demadrille, *Sustain. Energy Fuels*, 2021, **5**, 144-153.
- [16] S. Aghazada, M. K. Nazeeruddin, *Inorganics*, 2018, **6**, article no. 52.
- [17] T. Higashino, H. Imahori, *Dalton Trans.*, 2014, **44**, 448-463.
- [18] K. Kakiage, Y. Aoyama, T. Yano, K. Oya, J. Fujisawa, M. Hanaya, *Chem. Commun.*, 2015, **51**, 15894-15897.
- [19] P. S. Chandrasekhar, P. K. Parashar, S. K. Swami, V. Dutta, V. K. Komarala, *Phys. Chem. Chem. Phys.*, 2018, **20**, 9651-9658.
- [20] J.-M. Ji, H. Zhou, Y. K. Eom, C. H. Kim, H. K. Kim, *Adv. Energy Mater.*, 2020, **10**, article no. 2000124.
- [21] K. Zhang, C. Qin, X. Yang, A. Islam, S. Zhang, H. Chen, L. Han, *Adv. Energy Mater.*, 2014, **4**, article no. 1301966.
- [22] W. Naim, V. Novelli, I. Nikolinakos, N. Barbero, I. Dzeba, F. Grifoni, Y. Ren, T. Alnasser, A. Velardo, R. Borrelli, S. Haacke, S. M. Zakeeruddin, M. Graetzel, C. Barolo, F. Sauvage, *JACS Au*, 2021, **1**, 409-426.
- [23] T. Ono, T. Yamaguchi, H. Arakawa, *Sol. Energy Mater. Sol. Cells*, 2009, **93**, 831-835.
- [24] W. Ghann, H. Kang, E. Emerson, J. Oh, T. Chavez-Gil, F. Nesbitt, R. Williams, J. Uddin, *Inorganica Chim. Acta*, 2017, **467**, 123-131.
- [25] K. Funabiki, H. Mase, A. Hibino, N. Tanaka, N. Mizuhata, Y. Sakuragi, A. Nakashima, T. Yoshida, Y. Kubota, M. Matsui, *Energy Environ. Sci.*, 2011, **4**, 2186-2192.
- [26] C. Qin, Y. Numata, S. Zhang, X. Yang, A. Islam, K. Zhang, H. Chen, L. Han, *Adv. Funct. Mater.*, 2014, **24**, 3059-3066.
- [27] F. M. Jradi, X. Kang, D. O'Neil, G. Pajares, Y. A. Getmanenko, P. Szymanski, T. C. Parker, M. A. El-Sayed, S. R. Marder, *Chem. Mater.*, 2015, **27**, 2480-2487.
- [28] A. K. Vats, A. Pradhan, S. Hayase, S. S. Pandey, *J. Photochem. Photobiol. A*, 2020, **394**, article no. 112467.
- [29] M. Urbani, M.-E. Ragoussi, M. K. Nazeeruddin, T. Torres, *Coord. Chem. Rev.*, 2019, **381**, 1-64.
- [30] T. Ikeuchi, H. Nomoto, N. Masaki, M. J. Griffith, S. Mori, M. Kimura, *Chem. Commun.*, 2014, **50**, 1941-1943.
- [31] A. Ogunsipe, D. Maree, T. Nyokong, *J. Mol. Struct.*, 2003, **650**, 131-140.
- [32] L. Yu, W. Shi, L. Lin, Y. Guo, R. Li, T. Peng, *Dyes Pigm.*, 2015, **114**, 231-238.
- [33] D. K. Muli, B. L. Carpenter, M. Mayukh, R. A. Ghiladi, D. V. McGrath, *Tetrahedron Lett.*, 2015, **56**, 3541-3545.
- [34] M. Ince, R. Kuboi, T. Ince, K. Yoshimura, D. Motoyoshi, M. Sonobe, R. Kudo, S. Mori, M. Kimura, T. Torres, *Sustain. Energy Fuels*, 2021, **5**, 584-589.
- [35] K. Sakamoto, S. Yoshino, M. Takemoto, K. Sugaya, H. Kubo, T. Komoriya, S. Kamei, S. Furukawa, *J. Porphy. Phthalocyanines*, 2015, **19**, 688-694.
- [36] G. d. I. Torre, C. G. Claessens, T. Torres, *Chem. Commun.*, 2007, 2000-2015.
- [37] K. Sakamoto, S. Yoshino, M. Takemoto, N. Furuya, *J. Porphy. Phthalocyanines*, 2013, **17**, 605-627.
- [38] K. U. Rao, K. Venkateswarlu, *Synlett*, 2018, **29**, 1055-1060.
- [39] V. K. Singh, P. Salvatori, A. Amat, S. Agrawal, F. De Angelis, M. K. Nazeeruddin, N. V. Krishna, L. Giribabu, *Inorganica Chim. Acta*, 2013, **407**, 289-296.
- [40] T. Keleş, Z. Biyiklioglu, E. Güzel, M. Nebioğlu, İ. Şişman, *Appl. Organomet. Chem.*, 2021, **35**, article no. e6076.
- [41] W. Shi, B. Peng, Y. Guo, L. Lin, T. Peng, R. Li, *J. Photochem. Photobiol. A*, 2016, **321**, 248-256.
- [42] M. E. Casida, C. Jamorski, K. C. Casida, D. R. Salahub, *J. Chem. Phys.*, 1998, **108**, 4439-4449.
- [43] F. Furche, R. Ahlrichs, *J. Chem. Phys.*, 2002, **117**, 7433-7447.
- [44] R. E. Stratmann, G. E. Scuseria, M. J. Frisch, *J. Chem. Phys.*, 1998, **109**, 8218-8224.
- [45] C. Van Caillie, R. D. Amos, *Chem. Phys. Lett.*, 1999, **308**, 249-255.
- [46] C. Van Caillie, R. D. Amos, *Chem. Phys. Lett.*, 2000, **317**, 159-164.
- [47] Y. Zhao, D. G. Truhlar, *Theor. Chem. Acc.*, 2008, **120**, 215-241.
- [48] G. Tunç, E. Güzel, İ. Şişman, V. Ahsen, G. Cárdenas-Jirón, A. G. Gürek, *New J. Chem.*, 2019, **43**, 14390-14401.
- [49] G. Cardenas-Jiron, M. Borges-Martínez, E. Sikorski, T. Baruah, *J. Phys. Chem. C*, 2017, **121**, 4859-4872.
- [50] R. Urzúa-Leiva, R. Pino-Rios, G. Cárdenas-Jirón, *Phys. Chem. Chem. Phys.*, 2019, **21**, 4339-4348.
- [51] V. Barone, M. Cossi, *J. Phys. Chem. A*, 1998, **102**, 1995-2001.
- [52] M. Cossi, N. Rega, G. Scalmani, V. Barone, *J. Comput. Chem.*, 2003, **24**, 669-681.
- [53] R. L. Martin, *J. Chem. Phys.*, 2003, **118**, 4775-4777.
- [54] M. J. Frisch, G. W. Trucks, H. B. Schlegel, G. E. Scuseria, M. A. Robb, J. R. Cheeseman, G. Scalmani, V. Barone, B. Mennucci, G. A. Petersson, H. Nakatsuji, X. Li, M. Caricato, A. Marenich, J. Bloino, B. G. Janesko, R. Gomperts, B. Mennucci, H. P. Hratchian, J. V. Ortiz, A. F. Izmaylov, J. L. Sonnenberg, D. Williams-Young, F. Ding, F. Lipparini, F. Egidi, J. Goings, B. Peng, A. Petrone, T. Henderson, D. Ranasinghe, V. G. Zakrzewski, J. Gao, N. Rega, G. Zheng, W. Liang, M. Hada, M. Ehara, K. Toyota, R. Fukuda, J. Hasegawa, M. Ishida, T. Nakajima, Y. Honda, O. Kitao, H. Nakai, T. Vreven, K. Throssell, J. A. Montgomery Jr., J. E. Peralta, F. Ogliaro, M. Bearpark, J. J. Heyd, E. Brothers, K. N. Kudin, V. N. Staroverov, T. Keith, R. Kobayashi, J. Normand, K. Raghavachari, A. Rendell, J. C. Burant, S. S. Iyengar, J. Tomasi, M. Cossi, J. M. Millam, M. Klene, C. Adamo, R. Cammi, J. W. Ochterski, R. L. Martin, K. Morokuma, O. Farkas, J. B. Foresman, D. J. Fox, *Gaussian 09, Revision A.02*, Gaussian, Inc., Wallingford, CT, 2016.
- [55] QuantumATK, Version Q-2020.09, Synopsys QuantumATK.
- [56] J. P. Perdew, K. Burke, M. Ernzerhof, *Phys. Rev. Lett.*, 1996, **77**, 3865-3868.
- [57] J. P. Perdew, K. Burke, M. Ernzerhof, *Phys. Rev. Lett.*, 1997, **78**, 1396.
- [58] R. Gershoni-Poranne, A. Stanger, *Chem. Soc. Rev.*, 2015, **44**, 6597-6615.
- [59] K. Wolinski, J. F. Hinton, P. Pulay, *J. Am. Chem. Soc.*, 1990, **112**, 8251-8260.
- [60] D. Sundholm, H. Fliegl, R. J. Berger, *Wiley Interdiscip. Rev. Comput. Mol. Sci.*, 2016, **6**, 639-678.
- [61] C. F. Matta, R. J. Boyd, *The Quantum Theory of Atoms in Molecules: From Solid State to DNA and Drug Design*, John Wiley & Sons, 2007.

- [62] Z. Chen, C. S. Wannere, C. Corminboeuf, R. Puchta, P. V. R. Schleyer, *Chem. Rev.*, 2005, **105**, 3842-3888.
- [63] R. Báez-Grez, L. Ruiz, R. Pino-Rios, W. Tiznado, *RSC Adv.*, 2018, **8**, 13446-13453.
- [64] R. Pino-Rios, G. Cárdenas-Jirón, W. Tiznado, *Phys. Chem. Chem. Phys.*, 2020, **22**, 21267-21274.
- [65] R. Islas, T. Heine, G. Merino, *Acc. Chem. Res.*, 2012, **45**, 215-228.
- [66] T. A. Keith, *TK Gristmill Software, Version 19.02.13*, AIMAll, Overland Park, KS, USA, 2019, <http://aim.tkgristmill.com>.
- [67] E. W. Bethel, H. Childs, C. Hansen, *High Performance Visualization: Enabling Extreme-Scale Scientific Insight*, CRC Press, 2012.
- [68] F. Feixas, E. Matito, J. Poater, M. Solà, *Chem. Soc. Rev.*, 2015, **44**, 6434-6451.
- [69] E. Matito, *Phys. Chem. Chem. Phys.*, 2016, **18**, 11839-11846.
- [70] M. Giambiagi, M. S. de Giambiagi, K. C. Mundim, *Struct. Chem.*, 1990, **1**, 423-427.
- [71] J. Poater, X. Fradera, M. Duran, M. Solà, *Chem. Eur. J.*, 2003, **9**, 400-406.
- [72] J. Kruszewski, T. Krygowski, *Tetrahedron Lett.*, 1972, **13**, 3839-3842.
- [73] T. Lu, F. Chen, *J. Comput. Chem.*, 2012, **33**, 580-592.
- [74] A. G. Martynov, J. Mack, A. K. May, T. Nyokong, Y. G. Gorbunova, A. Y. Tsivadze, *ACS Omega*, 2019, **4**, 7265-7284.
- [75] X. Zarate, E. Schott, T. Gomez, R. Arratia-Pérez, *J. Phys. Chem. A*, 2013, **117**, 430-438.
- [76] X.-F. Zhang, Q. Xi, J. Zhao, *J. Mater. Chem.*, 2010, **20**, 6726-6733.
- [77] W. G. Touw, B. van Beusekom, J. M. G. Evers, G. Vriend, R. P. Joosten, *Acta Crystallogr. D*, 2016, **72**, 1110-1118.
- [78] S. Manzhos, G. Giorgi, K. Yamashita, *Molecules*, 2015, **20**, 3371-3388.
- [79] S. A. Haque, E. Palomares, B. M. Cho, A. N. M. Green, N. Hirata, D. R. Klug, J. R. Durrant, *J. Am. Chem. Soc.*, 2005, **127**, 3456-3462.
- [80] R. Katoh, A. Furube, M. Kasuya, N. Fuke, N. Koide, L. Han, *J. Mater. Chem.*, 2007, **17**, 3190-3196.
- [81] B. Ghazal, K. Azizi, E. F. Ewies, A. S. A. Youssef, V. M. Mwalukuku, R. Demadrille, T. Torres, S. Makhseed, *Molecules*, 2020, **25**, article no. E1692.